

# Anomalous Adverse Effect of Mass Velocity on Convective Flow Boiling in Small-Diameter Microfin Tubes

Lingnan Lin<sup>1</sup>

Mem. ASME

National Institute of Standards and Technology,  
100 Bureau Drive,  
Gaithersburg, MD 20899  
e-mail: lingnan.lin@nist.gov

Mark A. Kedzierski

Fellow ASME

National Institute of Standards and Technology,  
100 Bureau Drive,  
Gaithersburg, MD 20899  
e-mail: mak@nist.gov

*Recent studies report an anomalous phenomenon, particularly for small diameter microfin tubes, where the flow boiling heat transfer coefficient decreases with increasing mass velocity in the convective regime, which is contrary to that found for smooth tubes and larger diameter microfin tubes. This paper presents a critical literature review and mechanistic analysis of the anomalous phenomenon. Our analysis suggests that the anomalous phenomenon is a result of the transition of annular flow pattern from “flooded-groove” (film thickness > fin height) to “in-groove” (film thickness < fin height). The latter is associated with lower degree of turbulence, smaller wetted area, and therefore smaller heat transfer coefficient than the former. We speculated that the in-groove annular flow only occurs for small diameter tubes where the liquid film is relatively uniform, while larger tubes tend to remain flooded at the tube-bottom until dryout. This may explain the tendency of the anomalous phenomenon to occur in small diameter tubes.*

[DOI: 10.1115/1.4056569]

*Keywords:* flow boiling, microfin, small diameter, flow pattern, convective regime

## Introduction

The microfin tube is the most common enhanced tube that provides a significant heat transfer augmentation with relatively low pressure drop penalty [1]. Since its introduction in the 1970s, the microfin tube has been extensively used in heat exchangers for the HVAC and refrigeration industry. Virtually all air-cooled residential air conditioners use microfin tubes [1]. Manufacturers are capable of large-scale production of microfin tubes in various fin layouts and shapes with high precision. However, the advancement of manufacturing technologies vastly outpaced the fundamental understanding of the flow and heat transfer within microfin tubes, which in turn hinders the further development of high-performance microfin tubes and heat exchangers.

Flow boiling characteristics in microfin tubes have been studied for more than 30 years, but the underlying mechanisms are still not fully understood. Besides increasing the surface area for heat exchange, the presence of microfins alters the two-phase flow pattern and complicates the heat transfer process. The axial rifling of the microfins induces a spiraling secondary flow, which enhances the turbulence and encourages the annular flow regime to occur at lower vapor qualities [2]. The capillary wicking of the liquid within microgrooves enhances the heat transfer in the stratified flow regime by enlarging the wetted area [2–4], and it also contributes to the earlier transition from stratified flow to annular flow [2,5,6]. In addition, the narrow grooves between the microfins may shield nucleation sites from the flow and mitigate the nucleate boiling suppression [7,8]. Due to the distinct flow and heat transfer behaviors, the trends of the heat transfer coefficient (HTC) in microfin tubes with respect to key operating parameters such as heat flux ( $q$ ), mass velocity ( $G$ ), and vapor quality ( $x$ ) are

often quite different with and more complex than that in smooth tubes [9,10].

Recent studies report that the microfin-tube flow boiling heat transfer coefficient does not increase, and at times, even decreases with increasing mass velocity in the convective regime, which is generally known to exist in the high-quality region and under low-heat-flux conditions. This observation is contrary to that commonly made for smooth tubes and that made in earlier studies for microfin tubes. It is also counterintuitive at first glance because an increase in mass velocity typically enhances the convection and therefore the heat transfer efficiency. Although some explanations have been provided in the existing studies, this anomalous phenomenon is still poorly understood. In what follows, a critical literature review is provided, followed by an in-depth analysis and discussion of the observed characteristics and possible mechanisms. The scope of the present discussion is restricted to oil-free refrigerants in horizontal tubes only.

## Literature Review

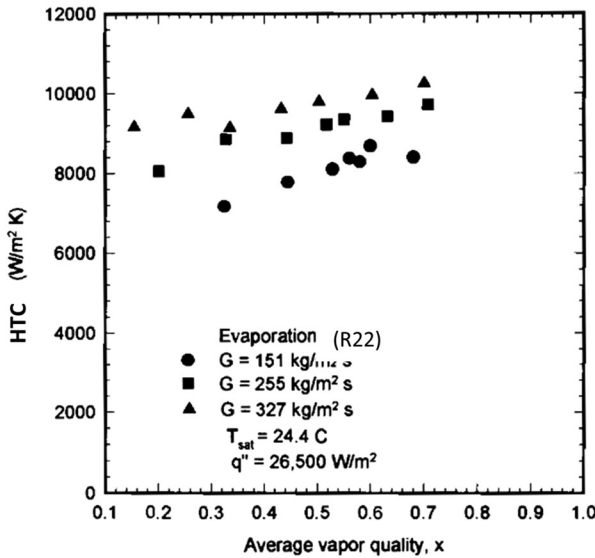
Comprehensive reviews on microfin tubes have been provided by Thome [9], Newell and Shah [10], and Webb and Kim [1], which are focused on studies before 2003. Since then, a multitude of studies on the flow boiling inside microfin tubes has been published. Most of these studies are concerned with low global-warming-potential refrigerants (e.g., CO<sub>2</sub> and hydrofluoroolefins (HFOs)) and smaller diameter tubes. The present review does not aim to provide an exhaustive publication list but instead focuses on studies that investigate the effect of  $G$  on HTCs in the predryout, convective flow boiling regime. The convective boiling regime is for  $x$  greater than that where the HTC is influenced by bubble nucleation. These conditions are identified by the increasing trend of HTC with respect to  $x$ , which are typically seen in conditions of high vapor quality (typically  $x > 0.5$ ) and low heat flux (typically  $q < 15 \text{ kW/m}^2$ ). Predryout region is identified by the range of  $x$  before the HTC dramatically drops as a result of the liquid film starting to dry out around the tube circumference (i.e., partial dryout).

The existing microfin-tube flow boiling literature may be divided into two groups regarding the trend of HTC with respect to  $G$ . In the first group, the convective HTCs monotonically

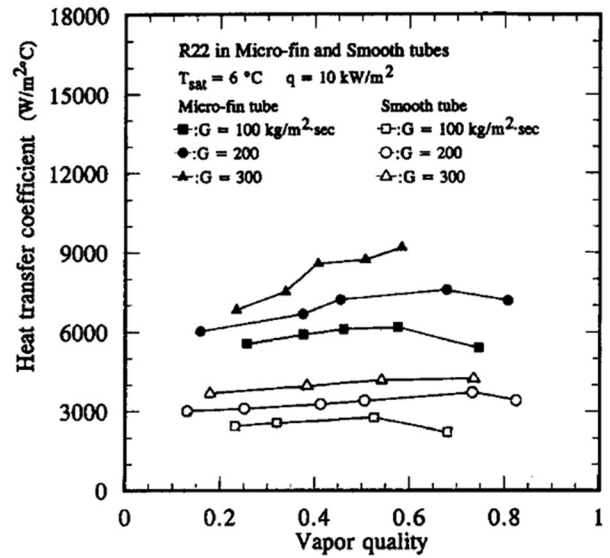
<sup>1</sup>Corresponding author.

Contributed by the Heat Transfer Division of ASME for publication in the JOURNAL OF HEAT AND MASS TRANSFER. Manuscript received July 20, 2022; final manuscript received December 15, 2022; published online February 21, 2023. Assoc. Editor: Anthony M. Jacobi.

This material is declared a work of the U.S. Government and is not subject to copyright protection in the United States. Approved for public release; distribution is unlimited.

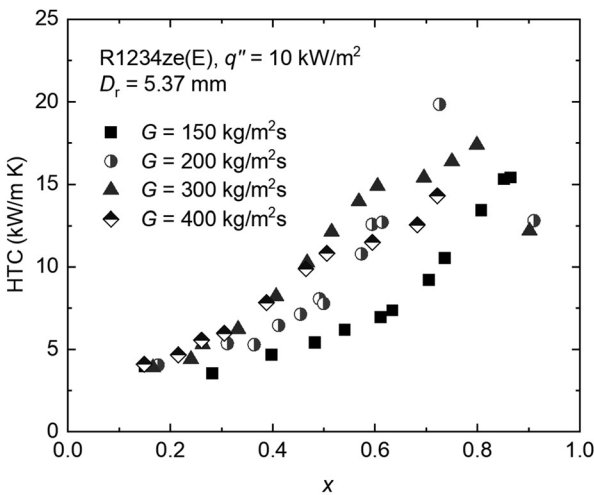


(a)

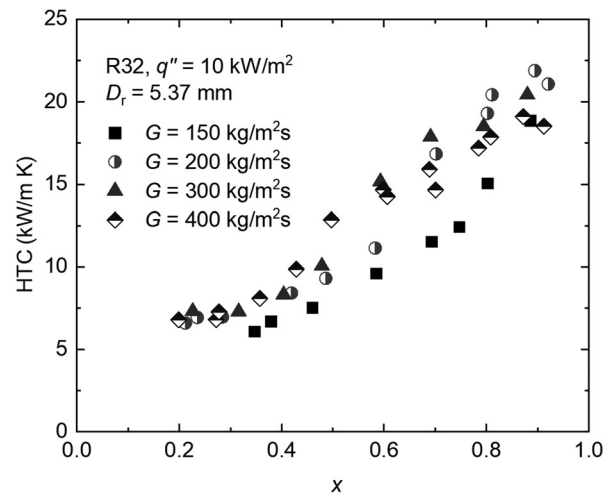


(b)

Fig. 1 Flow boiling measurements in smooth and microfin tubes with increasing trends of HTC with respect to increasing  $G$ : (a) a microfin tube with  $D_r = 14.66$  mm (from Ref. [11]) and (b) a microfin tube with  $D_r = 8.92$  mm and a 7.92 mm smooth tube (from Ref. [12])



(a)



(b)

Fig. 2 Replot of the flow boiling HTC data of microfin tubes by Baba et al. [16]

increase with the increase in  $G$ . Figure 1 shows two example sets of measurements with this trend [11,12]. The increasing trend of HTC with  $G$  is similar to that in smooth tubes and can be explained by the enhanced forced convection, the transition of flow pattern to (semi-) annular flow, and the reduced annular-film thickness with continuous increase in  $G$  [11].

In the second group of literature, the HTC in convective boiling regime are found not necessarily to increase with the increasing  $G$ ; instead, the HTCs decrease with  $G$ , especially when  $G$  is large. This trend was first observed in some  $\text{CO}_2$  measurements (e.g., Refs. [13] and [14]). However, these  $\text{CO}_2$  measurements are considered to have a large portion of, if not be dominated by, nucleate boiling, which is evident by the nearly flat trend of HTC versus  $x$ . Many studies have shown that flow boiling of  $\text{CO}_2$  is generally dominated by nucleate boiling, due to the relatively high reduced pressure and thereby low surface tension and high vapor density, which are conducive to bubble nucleation [15].

Thus, it is reasonable to consider the adverse effect of  $G$  seen in  $\text{CO}_2$  flow boiling as partly due to the suppression of nucleate boiling.

The “anomalous” behavior in this paper refers to the non-increasing trend of HTC with increasing  $G$  under conditions where the heat transfer mechanisms are apparently dominated by forced convection. This anomalous behavior, perhaps for the first time, is shown for the R1234ze(E) and R32 measurements of Baba et al. [16], although it is not discussed or noted in Ref. [16]. The Baba et al. [16] measurements are for a  $D_r = 5.37$  mm microfin tube, which is heated by water counterflowing in annulus tubes. Some of the measurements are replotted in Figs. 2(a) and 2(b). The selected measurements for  $x > 0.4$  are in the convective boiling regime, evident by the upward trend of HTC versus  $x$ . As shown in Figs. 2(a) and 2(b), convective HTCs of both R1234ze(E) and R32 increase with increasing  $G$  when  $G \leq 200$  kg/m<sup>2</sup>s, while the trend is reversed with further increase in  $G$ . Although the

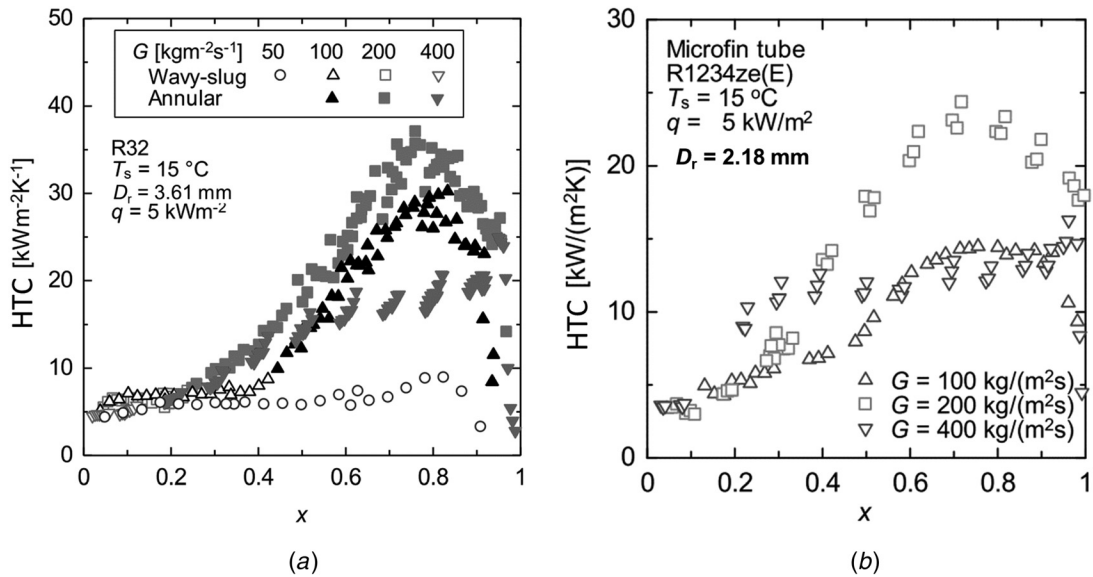


Fig. 3 Anomalous flow boiling HTC data of microfin tubes by Jige et al.: (a) R32 [17] and (b) R1234ze(E) [18]

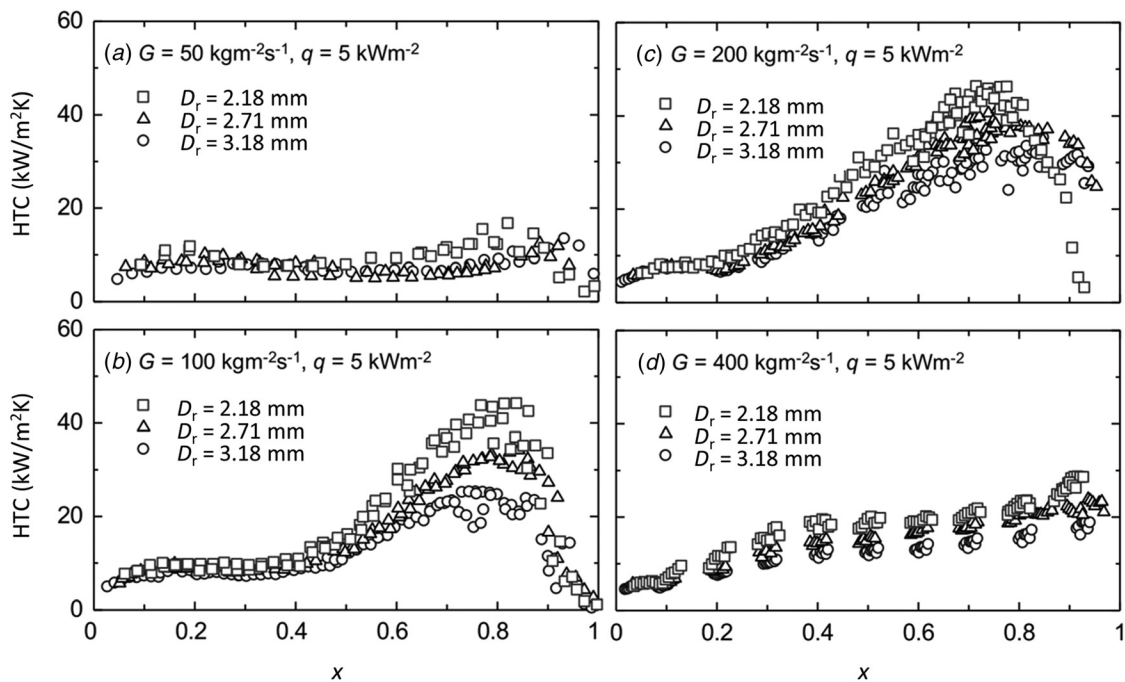


Fig. 4 Anomalous flow boiling HTC data of microfin tubes by Jige et al. for different tube diameters (adapted from Ref. [19])

difference between the HTC for  $G$  from  $200 \text{ kg/m}^2\text{s}$  to  $400 \text{ kg/m}^2\text{s}$  are small for R32, it is rather significant for R1234ze(E). Interestingly, the  $\text{HTC}-x$  slopes (i.e.,  $\partial h/\partial x$ ) are different for lower and higher  $G$ . For  $G = 150 \text{ kg/m}^2\text{s}$  or  $200 \text{ kg/m}^2\text{s}$ , the slope at higher  $x$  is greater than that at lower  $x$ . In contrast, for  $G = 300 \text{ kg/m}^2\text{s}$  or  $400 \text{ kg/m}^2\text{s}$ , the slope is smaller in high- $x$  region (i.e.,  $x$  approximately higher than 0.6) than that in medium- $x$  region (i.e.,  $x$  approximately between 0.4 and 0.6).

Jige et al. [17] report the anomalous adverse effect of  $G$  occurring during convective flow boiling of R32 in a microfin tube with  $D_r = 3.61 \text{ mm}$ , as shown in Fig. 3(a). The test tube is heated by Joule heating with an AC power supply. The end of the test tube is inserted into a glass tube for observation of adiabatic flow

pattern. As shown in Fig. 3(a), the data for  $x > 0.5$  and  $G$  of  $100 \text{ kg/m}^2\text{s}$ ,  $200 \text{ kg/m}^2\text{s}$ , and  $400 \text{ kg/m}^2\text{s}$  are annular flows, of which the HTCs are significantly larger than that of wavy-slug flows (i.e.,  $G = 50 \text{ kg/m}^2\text{s}$ ). Regarding the predryout region (i.e., before HTC drops dramatically at very high  $x$ ), the HTC increases as  $G$  increases from  $100 \text{ kg/m}^2\text{s}$  to  $200 \text{ kg/m}^2\text{s}$  but decreases significantly (i.e., by approximately 50%) as  $G$  further increases to  $400 \text{ kg/m}^2\text{s}$ . Similar trends are reported in R1234ze(E) flow boiling in a  $D_r = 2.18 \text{ mm}$  microfin tube [18] (Fig. 3(b)), and R32 flow boiling in microfin tubes with  $D_r$  of 2.18 mm, 2.71 mm, and 3.18 mm [19] (Fig. 4). Jige and Inoue [19] argue that the initial increase of HTC with  $G$  when  $G$  is relatively low is due to the enhancement by forced convection and evaporative heat transfer

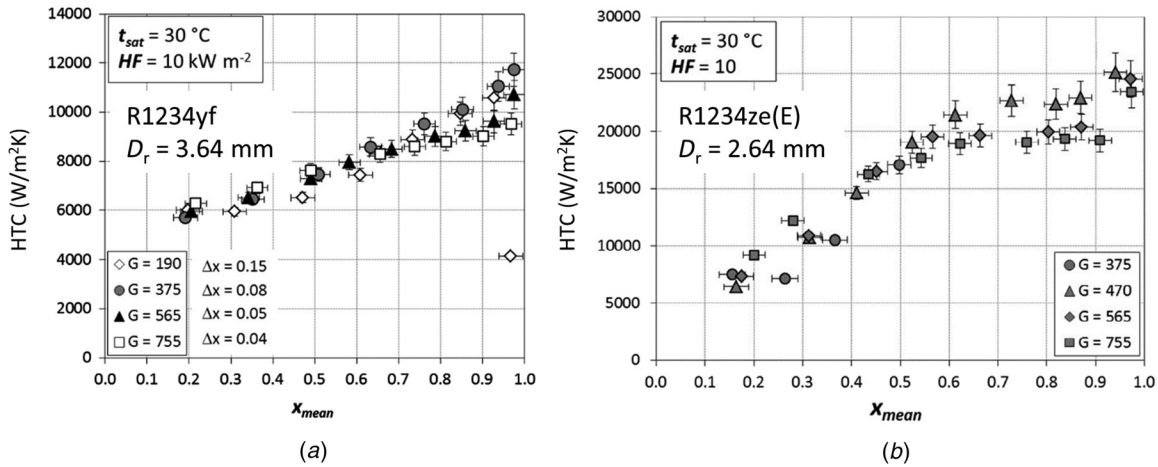


Fig. 5 Selected anomalous flow boiling HTC data of microfin tubes by Diani et al.: (a) from Ref. [21] and (b) from Ref. [23]

through the “meniscus liquid film” in the spiral grooves, while the adverse effect of further increase in  $G$  is because “the liquid film flows over the spiral grooves and there is no meniscus liquid film as the vapor shear stress further increases.”

Similar anomalous trends are also reported in a series of flow boiling studies performed at the University of Padova, Italy [20–29]. The test refrigerants include R134a and several HFO refrigerants. The  $D_r$  of microfin tubes range from 2.64 mm to 4.54 mm. Some of the results are shown in Fig. 5. In one of their earlier papers, Diani et al. [23] attribute the phenomenon to the possible suppression of nucleate boiling; however, in a more recent paper, Diani et al. [30] adopt the explanation by Jige and Inoue [19] that the liquid film breaks up over the fin tips as the vapor shear stress further increases. Righetti et al. [27] provide another explanation: the drop in saturation temperature as a result of the higher pressure drop associated with higher  $G$ .

Table 1 summarizes the above two groups of literature in terms of the trend of HTC versus  $G$ , the test fluid, the microfin geometry (fin-root diameter  $D_r$ , helix angle  $\alpha$ , apex angle  $\beta$ , fin height  $e$ , number of fins  $N_f$ ), the operating conditions, and the heating condition (i.e., electric or fluid heating). Measurements for  $\text{CO}_2$  are not taken into account due to the large nucleate boiling contribution, as discussed previously. Original values of heat flux, mass velocity, and HTC from the literature are used in this paper unless otherwise noted. Although existing papers use different base area definitions to reduce data for these parameters, the resulting deviation is generally within  $\pm 10\%$ , which does not severely affect the discussion hereafter, as we do not cross-compare the parameters among the literature.

Figure 6 shows the two groups of literature in terms of the inside tube diameter and fin height of their tested microfin tubes. The anomalous behavior has been observed for various fluids, including high-pressure refrigerants such as R32 and medium pressure refrigerants such as R134a and R1234yf. Interestingly, the anomalous adverse effect of  $G$  on convective HTCs only appears in microfin tubes with  $D_r < 5.5$  mm, whereas larger diameter tubes tend to have normal trends (HTC increases with increasing  $G$ ). However, this is not to say that  $D_r = 5.5$  mm is a threshold below which the anomalous adverse effect will occur, as there are two studies [41,44] showing normal trends for  $D_r$  of approximately 4.6 mm.

## Analysis and Discussion

The convective flow boiling within smooth tubes is often associated with annular flow pattern, where the heat is transferred through a thin liquid film and the evaporation occurs at the interface of the liquid film and the vapor core [47]. The convection

within the liquid film constitutes the main resistance to heat transfer, which is essentially flow dependent. An increase in the mass velocity will enhance the convection within the film and meanwhile reduce the film thickness, and consequently increase the HTC.

For microfin tubes, annular flow occurs at lower vapor quality and mass velocity and lasts for a wider range of vapor quality, largely due to the capillary and momentum forces imposed on the liquid within the helical grooves [2,33,48]. Thus, the flow pattern in convective boiling region for microfin tubes is most likely to be annular flow. The visualization results by Jige et al. [17] confirm that the reported anomalous phenomenon (i.e., a larger mass velocity is associated with smaller HTC) occurred in the annular flow regime. Therefore, the following discussion will be restricted to the annular flow pattern.

It is reasonable to expect that the flow and heat transfer characteristics of annular flows in microfin tubes can differ when the liquid film thickness ( $\delta$ ) is larger or smaller than the height of microfins ( $e$ ). When  $\delta > e$ , the microfins and grooves are flooded by the annular liquid film. This pattern is referred to as the *flooded-groove* annular flow as opposed to the *in-groove* annular flow pattern (i.e.,  $\delta < e$ ). For flooded-groove annular flow, a swirling liquid flow exists within the flooded grooves due to the helical layout of microfins, while the liquid flow above the grooves and near the liquid–vapor interface is largely aligned with the axial vapor flow (Fig. 7). The superposition of the main axial flow and the secondary swirling flow involves intense fluid mixing and momentum/heat transfer. Besides inducing secondary flows, the microfins also trip the liquid film in the axial direction, inducing flow separation and re-attachment (Fig. 8), similar to that occurring in single-phase flow where the microfin acts like a roughness [1,49]. In addition, liquid films that are thicker than the height of microfins allow the disturbance waves to freely propagate axially and circumferentially, which plays an important role in maintaining the annular flow [50,51]. The combination of the above effects is believed to be associated with a very high degree of turbulence. Therefore, enhanced heat transfer can be expected for the flooded-groove annular flow ( $\delta > e$ ).

When  $\delta < e$ , the microfins protrude through the thin liquid film, dividing the annular liquid film into smaller films that flow within the grooves, as shown in Fig. 9. This pattern is referred to as the *in-groove* annular flow pattern. The liquid films in this flow pattern are largely driven by inertial and capillary forces to reach the top of the tube, which is quite different from the mechanism in flooded-groove annular flow where the liquids films are largely driven by disturbance waves [50,51]. The turbulence in the in-groove pattern is considered to be reduced significantly as the microfins no longer act as “roughness”; instead, they are

**Table 1 Summary of the reviewed literature about flow boiling of microfin tubes**

| Authors (year)  | References <sup>a</sup> | Fluid                               | HTC trend <sup>b</sup>   | $x$       | $q$ (kW/m <sup>2</sup> ) | $G$ (kg/m <sup>2</sup> s) | $T$ (°C) | $D_r$ (mm) | $\alpha$ (deg) | $\beta$ (°) | $e$ (mm) | $N_f$  | H <sup>c</sup> |
|---|-------------------------|-------------------------------------|--|-----------|--------------------------|---------------------------|----------|------------|----------------|-------------|----------|--------|----------------|
| <i>Group 1: HTC's monotonically increase with increasing <math>G</math></i> |                         |                                     |  |           |                          |                           |          |            |                |             |          |        |                |
| Schlager et al. (1989)  | [3], Fig. 7             | R22                                 | Increasing   | n/a       | n/a                      | 180–400                   | n/a      | 8.92       | 18,15,25       | n/a         | 0.3      | 60     | F              |
| Chamra and Webb (1995)  | [11], Fig. 9            | R22                                 | Increasing   | 0.1–0.7   | 26.5                     | 151–327                   | 24.4     | 14.66      | 15             | n/a         | 0.35     | 74     | F              |
| Kuo and Wang (1996)   | [12], Fig. 8            | R22                                 | Increasing   | 0.2–0.8   | 10                       | 100–300                   | 6        | 8.92       | 18             | n/a         | 0.2      | 60     | F              |
| Lallemand et al. (2001)   | [31], Fig. 3            | R22                                 | Increasing   | 0.1–1.0   | 10                       | 100–250                   | 14       | 11.98      | 20, 30         | 40, 50      | 0.25     | 65, 70 | E              |
| Kim et al. (2002)   | [32], Fig. 10           | R410A                               | Increasing   | 0.2–0.8   | 5                        | 117–211                   | –5       | 6.46       | 18             | n/a         | 0.15     | 60     | F              |
| Kim et al. (2002)   | [32], Fig. 10           | R410A                               | Increasing   | 0.2–0.8   | 5                        | 70–164                    | –5       | 8.92       | 25             | n/a         | 0.12     | 60     | F              |
| Yu et al. (2002)  | [33], Fig. 3a           | R134a                               | Increasing   | 0–0.7     | 2.2–56                   | 163–408                   | 6        | 11.1       | 18             | n/a         | 0.3      | 60     | E              |
| Wongsa-Ngam et al. (2004)   | [34], Fig. 4b           | R134a                               | Increasing   | 0.2–0.8   | 10                       | 400–800                   | 10–15    | 8.92       | 18             | n/a         | 0.20     | 60     | E              |
| Spindler and Müller-Steinhagen (2009)                                       | [35], Fig. 9            | R134a                               | Increasing   | n/a       | 1–15                     | 20–150                    | –20      | 8.92       | 15             | 20          | 0.24     | 55     | E              |
| Bandarra Filho et al. (2011)  | [36], Figs. 6–8         | R134a                               | Increasing   | 0.1–0.5   | 3                        | 101–506                   | 5        | 8.92       | 18             | n/a         | 0.20     | 60     | E              |
| Padovan et al. (2011)   | [37], Fig. 3            | R134a                               | Increasing   | 0.1–0.9   | 15                       | 80–200                    | 30       | 8.15       | 13             | 43          | 0.23     | 60     | F              |
| Han et al. (2013)   | [38], Fig. 10           | R22, R161                           | Increasing   | 0.1–0.8   | 18–32                    | 100–250                   | 8        | 6.41       | 15             | 34          | 0.10     | 65     | E              |
| Kondou et al. (2013)  | [39], Fig. 8a           | R1234ze(E)                          | Increasing   | 0.2–0.6   | 10                       | 190, 352                  | 10       | 5.45       | 20             | 18          | 0.26     | 48     | F              |
| Kondou et al. (2013)  | [39], Fig. 8d           | R32                                 | Increasing   | 0.2–0.8   | 10                       | 191, 382                  | 10       | 5.45       | 20             | 18          | 0.26     | 48     | F              |
| Kondou et al. (2014)  | [40], Fig. 10           | R1234ze(Z),<br>R134a,<br>R1234ze(E) | Increasing   | 0.20–0.98 | 10                       | 150, 300                  | 30       | 5.45       | 20             | 18          | 0.26     | 48     | F              |
| Kim (2015)  | [41], Fig. 13a          | R410A                               | Increasing   | 0.2–0.6   | 15                       | 260–433                   | 10       | 4.67       | 18             | 40          | 0.15     | 40     | F              |
| Jiang et al. (2016)   | [42], Fig. 6            | R410A,<br>R134a, R22                | Increasing   | 0.10–0.90 | 3–14                     | 48–430                    | 5        | 8.96       | 18             | 66          | 0.14     | 60     | F              |
| Yang and Hrnjak (2018)  | [43], Fig. 8a           | R410A                               | Increasing   | 0.1–0.9   | 15                       | 100–450                   | 10       | 6.52       | 0              | ?           | 0.22     | 58     | F              |
| Kim (2019)  | [44], Fig. 12           | R410A                               | Increasing   | 0.2–0.8   | n/a                      | 50–250                    | 8        | 4.6        | 18             | 40          | 0.15     | 40     | F              |
| Kim (2019)  | [44], Fig. 12           | R410A                               | Increasing   | 0.2–0.8   | n/a                      | 50–250                    | 8        | 6.56       | 15             | 40          | 0.1      | 40     | F              |
| Colombo et al. (2020)   | [45], Fig. 4            | R1234ze(E)                          | Increasing   | 0.2–0.8   | 10–16.5                  | 163–220                   | 5–45     | 8.96       | 18             | 40          | 0.2      | 60     | F              |
| <i>Group 2: HTC's potentially decrease with increasing <math>G</math></i>   |                         |                                     |  |           |                          |                           |          |            |                |             |          |        |                |
| Baba et al. (2012)  | [16], Fig. 3            | R1234ze(E)                          | Increasing for<br>$G \leq 200$ , decreasing<br>for $G > 200$             | 0.5–0.9   | 10                       | 150–400                   | 10       | 5.37       | 19             | n/a         | 0.26     | 58     | F              |
| Baba et al. (2012)  | [16], Fig. 4            | R32                                 | Increasing for<br>$G \leq 200$ , slightly<br>decreasing for<br>$G > 200$ | 0.6–0.9   | 10                       | 150–400                   | 10       | 5.37       | 19             | n/a         | 0.26     | 58     | F              |
| Diani et al. (2014)   | [20], Fig. 4            | R1234ze(E)                          | Decreasing   | 0.7–1     | 10                       | 190–755                   | 30       | 3.64       | 18             | 43          | 0.12     | 40     | E              |
| Diani et al. (2015)   | [21], Fig. 10a          | R1234yf,<br>R134a                   | Increasing for<br>$G \leq 375$ , decreasing<br>for $G > 375$             | 0.5–1     | 10                       | 375–565                   | 30       | 3.64       | 18             | 43          | 0.12     | 40     | E              |

Table 1 (continued)

| Authors (year)            | References <sup>a</sup> | Fluid          | HTC trend <sup>b</sup>  | $x$     | $q$ (kW/m <sup>2</sup> ) | $G$ (kg/m <sup>2</sup> s) | $T$ (°C) | $D_r$ (mm) | $\alpha$ (deg) | $\beta$ (°) | $e$ (mm) | $N_f$ | H <sup>c</sup> |
|---------------------------|-------------------------|----------------|---|---------|--------------------------|---------------------------|----------|------------|----------------|-------------|----------|-------|----------------|
| Diani and Rossetto (2015) | [22], Fig. 3            | R1234yf, R134a | Decreasing  | 0.5–1   | 10                       | 375–565                   | 30       | 2.64       | 7              | 43          | 0.12     | 40    | E              |
| Diani et al. (2016)       | [23], Fig. 4a           | R1234ze(E)     | Decreasing  | 0.5–1   | 10                       | 375–755                   | 30       | 2.64       | 7              | 43          | 0.12     | 40    | E              |
| Longo et al. (2017)       | [24], Fig. 4a           | R134a          | Not significantly increasing or decreasing                      | 0.5–0.9 | 15                       | 200–800                   | 30       | 4.54       | 27             | 11          | 0.12     | 54    | E              |
| Diani et al. (2017)       | [25], Fig. 4            | R1234yf        | Decreasing  | 0.6–1   | 10                       | 375–755                   | 30       | 2.64       | 7              | 43          | 0.12     | 40    | E              |
| Diani and Rossetto (2018) | [26], Fig. 3a           | R134a          | Decreasing  | 0.5–0.9 | 10                       | 375–755                   | 30       | 2.64       | 7              | 43          | 0.12     | 40    | E              |
| Righetti et al. (2018)    | [27], Fig. 5            | R1233zd(E)     | Increasing for $G \leq 200$ , decreasing for $G > 200$          | 0.5–0.9 | 15                       | 100–300                   | 30       | 4.54       | 27             | 11          | 0.12     | 54    | E              |
| Jige et al. (2018)        | [17], Fig. 8            | R32            | Increasing for $G \leq 200$ , decreasing for $G > 200$          | 0.5–0.8 | 5                        | 50–400                    | 15       | 3.61       | 17             | n/a         | 0.18     | 40    | E              |
| Jige et al. (2018)        | [18], Fig. 5            | R1234ze(E)     | Increasing for $G \leq 200$ , decreasing for $G > 200$          | 0.6–0.9 | 5                        | 100–400                   | 15       | 2.18       | 10             | n/a         | 0.10     | 25    | E              |
| Righetti et al. (2019)    | [46], Fig. 5a           | R1233zd(E)     | Increasing for $G \leq 200$ , slightly decreasing for $G > 200$ | 0.6–0.9 | 15                       | 100–300                   | 30       | 4.50       | 18             | 42          | 0.15     | 40    | E              |
| Righetti et al. (2019)    | [46], Fig. 7a           | R245fa         | Increasing for $G \leq 200$ , slightly decreasing for $G > 200$ | 0.6–0.9 | 15                       | 100–300                   | 30       | 4.50       | 18             | 42          | 0.15     | 40    | E              |
| Diani and Rossetto (2019) | [29], Fig. 6            | R513A          | Increasing for $G \leq 400$ , decreasing for $G > 400$          | 0.5–0.9 | 12                       | 150–800                   | 20       | 3.64       | 18             | 43          | 0.12     | 40    | E              |
| Diani and Rossetto (2020) | [30], Fig. 4b           | R513A          | Decreasing  | 0.5–0.9 | 12                       | 300–800                   | 20       | 2.64       | 7              | 43          | 0.12     | 40    | E              |
| Jige and Inoue (2019)     | [19], Fig. 4            | R32            | Increasing for $G \leq 200$ , decreasing for $G > 200$          | 0.5–0.9 | 5                        | 5–400                     | 15       | 2.18       | 10             | n/a         | 0.10     | 25    | E              |
| Jige and Inoue (2019)     | [19], Fig. 6            | R32            | Increasing for $G \leq 200$ , decreasing for $G > 200$          | 0.5–0.9 | 5                        | 5–400                     | 15       | 2.71       | 10             | n/a         | 0.11     | 25    | E              |
| Jige and Inoue (2019)     | [19], Fig. 6            | R32            | Increasing for $G \leq 200$ , decreasing for $G > 200$          | 0.5–0.9 | 5                        | 5–400                     | 15       | 3.18       | 11             | n/a         | 0.11     | 25    | E              |

<sup>a</sup>The figure number in this column refers to that in the original paper.

<sup>b</sup>Overall trend of heat transfer coefficient (HTC) with respect to mass velocity ( $G$ ).

<sup>c</sup>Heating method. E: electric heating; F: fluid heating.

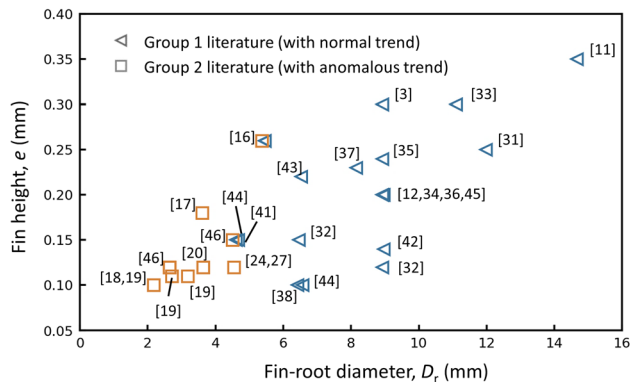


**Fig. 6** Reviewed literature classified into two groups based on whether the HTC trend is normal (i.e., monotonically increasing with increasing  $G$ ) or not. Each symbol refers to a specific paper in Table 1. The annotation in a bracket is the citation number of the corresponding paper.

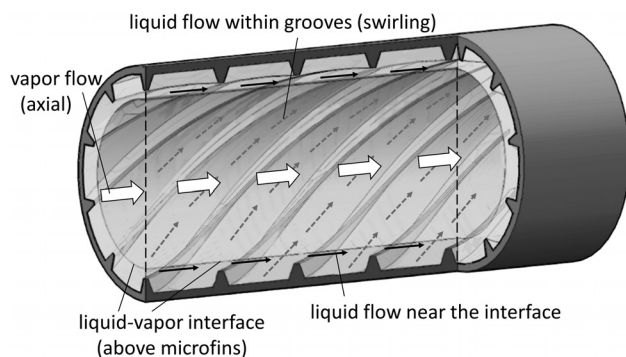


**Fig. 7** Illustration of the secondary swirling flow within the liquid film in the flooded-groove annular flow ( $\delta > e$ )

essentially smooth-walled channels that direct the liquid flow. Furthermore, the wetted area is reduced as the fin tips become dry when the liquid films are too thin to flood the microfins and grooves. Based on the above reasons, it is reasonable to expect a degraded HTC for the in-groove annular flow ( $\delta < e$ ).

For a certain vapor quality ( $x$ ), the film thickness is related to the void fraction ( $\epsilon$ ). Assuming uniform film thickness around the circumference and zero microfin thickness (or width), the relation between  $\delta$  and  $\epsilon$  for microfin tubes is the same as that for smooth tubes and can be written as [52]

$$\delta = \frac{1}{4}(1 - \epsilon)D_r \quad (1)$$

The void fraction is a function of the mass velocity, vapor quality, and fluid properties. A simple correlation for the void fraction in microfin tubes is proposed by Yashar et al. [53]

$$\epsilon = \left[ 1 + \left( \frac{G^2 x^3}{(1-x)\rho_v^2 g D_r} \right)^{-0.5} + X_{tt} \right]^{-0.321} \quad (2)$$

where  $X_{tt}$  is the Martinelli parameter. According to Eq. (2), an increase in  $G$  will increase the void fraction. A similar trend is observed by Koyama et al. [54]. Together from Eqs. (1) and (2), it can be expected that a higher  $G$  is associated with a smaller  $\delta$  in microfin tubes. Therefore, it is possible that for two annular flow conditions 1 and 2 where  $x_1 = x_2$  and  $G_1 < G_2$ , the liquid film in condition 1 is thicker than the microfins while that in condition 2 is thinner than the microfins, i.e.,  $\delta_1 > e > \delta_2$ . That is, as the  $G$

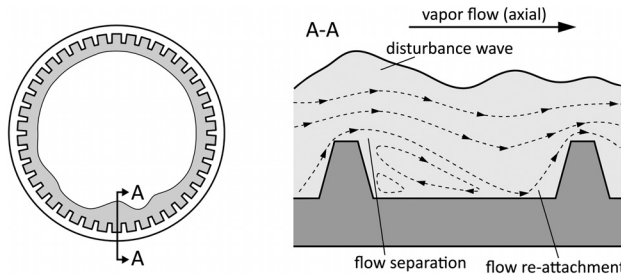


**Fig. 8** Flow separation and re-attachment within the liquid film in the flooded-groove annular flow ( $\delta > e$ )

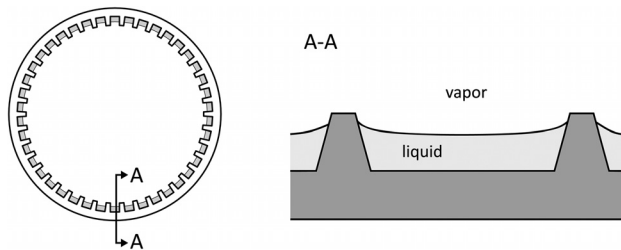


**Fig. 9** Illustration of the liquid film flowing within the grooves in the in-groove annular flow ( $\delta < e$ )

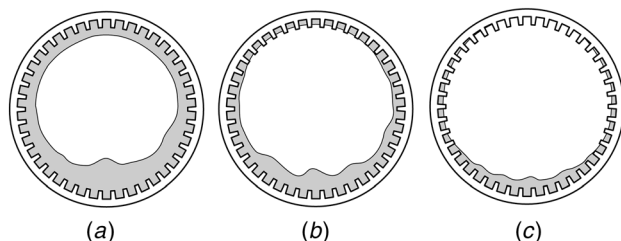


**Fig. 10** Illustration of different stages of flooded-groove annular flow pattern in large diameter microfin tubes: (a) at a smaller  $x$ , all fins and grooves are flooded and (b) at a higher  $x$ , some fin tips at the top of the tube are dry, while the fins and grooves at the bottom of the tube remain flooded; (c) as  $x$  continues to increase, the upper tube starts to dry out, while the lower tube remains flooded

increases from  $G_1$  to  $G_2$ , the flow pattern transitions from the flooded-groove ( $\delta > e$ ) to in-groove ( $\delta < e$ ) annular flow. Based on the earlier analysis, the HTC of the flooded-groove pattern is higher than that of the in-groove pattern, thus  $HTC_1 > HTC_2$ . This explains the anomalous phenomenon that an increase in  $G$  can have an adverse influence on the HTC of convective flow boiling in microfin tubes.

The thermophysical properties may also influence the flow pattern transition from the flood-groove to in-groove and therefore the adverse effect of  $G$ . As indicated by Eqs. (1) and (2), refrigerants with larger vapor density have lower void fraction and thicker liquid film for the same  $x$  and  $G$ . Thus, the flow pattern transition would occur later (i.e., at a higher  $x$ ) for these refrigerants. This may explain why in Fig. 2 the anomalous adverse effect of  $G$  is more significant for R1234ze(E) (smaller vapor density) than for R32 (larger vapor density).

An important assumption for the above analysis is uniform film distribution. This is considered a satisfactory approximation for small diameter tubes, where the effect of gravitational drainage is small and the annular films become more uniform in high vapor quality region [51]. For large diameter tubes, however, the film thickness at the bottom of the tube tends to be larger than that at

the sides and the top. In this case, we speculated that the bottom of the tube and parts of the sides remain flooded before the dryout occurs at the top of the tube, as schematically shown in Fig. 10 (note: the comparison of HTC for different  $G$  herein is limited to the predryout region, which corresponds to Figs. 10(a) and 10(b)). Consequently, an increase in  $G$  will always decrease the film thickness and enhance the convection within the liquid films that cover the microfins, which is associated with an increasing HTC. This explains the observation made in the section Literature Review that large microfin tubes generally exhibit monotonically increasing trend of HTC with respect to increasing  $G$  in the predryout, convection dominant regime, whereas small diameter tubes exhibit the “anomalous” opposite trend.

It is still unclear how a further increase in  $G$  will influence the heat transfer in the in-groove annular flow, i.e., when the film is uniform (e.g., in very small diameter tubes) and  $G$  exceeds a certain value such that the film thickness is smaller than the fin height (note: the fin height is generally between 0.1 and 0.15 mm for studies where this anomalous behavior was observed). The existing data are limited in this regard. Theoretically, an increase in  $G$  enhances the convection in both the vapor and the liquid phase and thins the liquid film, thereby enhances the heat transfer. On the other hand, the liquid film thinning also enlarges the dry area near the tips of the microfins, which penalizes the overall heat transfer. The overall heat transfer would therefore depend on the competition of these two effects. It is speculated that the trend of HTC with respect to increasing  $G$ , in this case, would be similar to that with respect to increasing  $x$  because either increasing  $G$  or  $x$  has a similar effect in enhancing the convection and decreasing the film thickness.

Another possible factor for the anomalous behavior is the heating method of the flow boiling experiments, i.e., electrically or fluid heating. All the studies that report the anomalous phenomenon except Ref. [16] were performed with electrically heated tubes (Table 1). However, electrically heating method may be relatively unreliable, particularly in conditions that involve (partial) dryout [55–57]. The main reason is that when an electrically heated tube is partially wetted, the boundary condition becomes neither uniform heat flux nor uniform temperature [55], and it will induce an axial wall conduction that affects the downstream flow and heat transfer characteristics [56]. As the anomalous phenomenon is thought to be related to the fin-tip drying out, fluid heating is more appropriate for heat transfer measurement than electrically heating. Thus, more tests with fluid heating should be carried out in the future to study the flow boiling characteristics in microfin tubes (in particular, with small diameters) and verify if the anomalous behavior persists for the fluid heated boundary condition. Although this work is focused on oil-free refrigerants, we expect the presence of oil would alter the flow behavior and may lead to different trends of HTC with respect to  $G$ . The oil effects should be considered in the future work. In addition, detailed visualization experiments are recommended for future studies to observe the in-groove annular flow pattern.

## Conclusions

Several existing studies have shown that an increase in mass velocity can anomalously decrease the flow boiling HTC in the convective regime, in particular for small diameter microfin tubes. Our analysis suggests that the anomalous behavior is a result of the transition of annular flow pattern from “flooded-groove” (film thickness  $>$  fin height) to “in-groove” (film thickness  $<$  fin height). The latter is associated with considerably lower degree of turbulence, smaller wetted area, and therefore smaller heat transfer coefficient than the former. As the mass velocity increases, the annular film thickness decreases; when the liquid film is thinner than the fin height, the flow transitions to the in-groove pattern with degraded heat transfer performance. The flow pattern transition may occur later (i.e., at a higher  $x$ ) for refrigerants with large vapor density, and the adverse effect of mass velocity may be less

significant for these refrigerants. We speculated that the in-groove annular flow only occurs in small diameter tubes where the liquid film is relatively uniform, while larger tubes tend to remain flooded at the bottom until dryout. This may explain the tendency of the anomalous phenomenon to occur in small diameter tubes. Future studies may use flow visualization experiments to validate the above analysis and elucidate the mechanisms. More flow and heat transfer measurements, especially with fluid heating and for small diameter tubes, are also needed.

## Acknowledgment

The authors thank Dr. Harrison Skye of NIST, Dr. Cheng-Min Yang of the Oak Ridge National Lab, and Dr. Donggyu Kang for the helpful discussion and constructive comments on the draft paper.

## Funding Data

- National Institute of Standards and Technology (NIST), United States (Funder ID: 10.13039/100000161).

## Data Availability Statement

The datasets generated and supporting the findings of this article are obtainable from the corresponding author upon reasonable request.

## Nomenclature

- $D_r$  = tube diameter at the fin root, m  
 $e$  = height of microfins, m  
 $G$  = mass velocity,  $\text{kg m}^{-2} \text{s}^{-1}$   
 $N_f$  = number of fins  
 $q$  = heat flux,  $\text{W m}^{-2}$   
 $T_{\text{sat}}$  = saturation temperature, K or  $^{\circ}\text{C}$   
 $x$  = vapor quality  
 $\alpha$  = helix angle, deg  
 $\beta$  = apex angle, deg  
 $\delta$  = film thickness, m  
 $\varepsilon$  = void fraction  
 $\rho$  = density,  $\text{kg m}^{-3}$

## Abbreviations

- HFO = hydrofluoroolefin  
 HTC = heat transfer coefficient

## References

- [1] Webb, R. L., and Kim, N.-H., 2005, *Principles of Enhanced Heat Transfer*, 2nd ed., Taylor & Francis, New York.
- [2] Yang, C. M., and Hrnjak, P., 2019, “Effect of Helical Micro-Fins on Two-Phase Flow Behavior of R410A Evaporating in Horizontal Round Tubes Obtained Through Visualization,” *Int. J. Heat Mass Transfer*, **144**, p. 118654.
- [3] Schlager, L., Pate, M., and Bergles, A., 1989, “Heat Transfer and Pressure Drop During Evaporation and Condensation of R22 in Horizontal Micro-Fin Tubes,” *Int. J. Refrig.*, **12**(1), pp. 6–14.
- [4] Kimura, H., and Ito, M., 1981, “Evaporating Heat Transfer in Horizontal Internal Spiral-Grooved Tubes in the Region of Low Flow Rates,” *Bull. JSME*, **24**(195), pp. 1602–1607.
- [5] Cavallini, A., Col, D. D., Rossetto, L., Tecnic, F., and Padova, U., 2006, “Flow Boiling Inside Microfin Tubes: Prediction of the Heat Transfer Coefficient,” ECI International Conference on Boiling Heat Transfer, Spoleto, Italy, May 7–12.
- [6] Liu, J., Liu, J., Zhang, L., and Xu, X., 2021, “Theoretical Analysis of Annular Film Flow Evaporation Inside Microfin Tube,” *Int. J. Heat Mass Transfer*, **165**, p. 120611.
- [7] Yang, C. M., and Hrnjak, P., 2020, “Diabatic Visualization Shows Effects of Micro-Fins on Evaporation of R410A: Smooth, Axial Micro-Fin, and Helical Micro-Fin Tubes,” *Int. J. Heat Mass Transfer*, **150**, p. 119276.
- [8] Thome, J. R., 1996, “Boiling of New Refrigerants: A State-of-the-Art Review,” *Int. J. Refrig.*, **19**(7), pp. 435–457.
- [9] Thome, J. R., 1999, “Flow Boiling Inside Microfin Tubes: Recent Results and Design Methods,” *Heat Transfer Enhancement of Heat Exchangers*, S. Kakaç,

- A. E. Bergles, F. Mayinger, and H. Yüncü, eds., Springer, Dordrecht, Netherlands, pp. 487–513.
- [10] Newell, T. A., and Shah, R. K., 2001, “An Assessment of Refrigerant Heat Transfer, Pressure Drop, and Void Fraction Effects in Microfin Tubes,” *HVAC&R Res.*, **7**(2), pp. 125–153.
- [11] Chandra, L. M., and Webb, R. L., 1995, “Condensation and Evaporation in Micro-Fin Tubes at Equal Saturation Temperatures,” *J. Enhanc. Heat Transfer*, **2**(3), pp. 219–229.
- [12] Kuo, C. S., and Wang, C. C., 1996, “In-Tube Evaporation of HCFC-22 in a 9.52 mm Micro-Fin/Smooth Tube,” *Int. J. Heat Mass Transfer*, **39**(12), pp. 2559–2569.
- [13] Schael, A.-E., and Kind, M., 2005, “Flow Pattern and Heat Transfer Characteristics During Flow Boiling of CO<sub>2</sub> in a Horizontal Micro Fin Tube and Comparison With Smooth Tube Data,” *Int. J. Refrig.*, **28**(8), pp. 1186–1195.
- [14] Dang, C., Haraguchi, N., and Hihara, E., 2010, “Flow Boiling Heat Transfer of Carbon Dioxide Inside a Small-Sized Microfin Tube,” *Int. J. Refrig.*, **33**(4), pp. 655–663.
- [15] Mastrullo, R., Mauro, A. W., and Viscito, L., 2019, “Flow Boiling of Carbon Dioxide: Heat Transfer for Smooth and Enhanced Geometries and Effect of Oil. State of the Art Review,” *Int. J. Refrig.*, **108**, pp. 311–335.
- [16] Baba, D., Nakagawa, T., and Koyama, S., 2012, “Flow Boiling Heat Transfer and Pressure Drop of R1234ze(E) and R32 in a Horizontal Micro-Fin Tube,” *International Refrigeration and Air Conditioning Conference*, West Lafayette, IN, July 16–19, p. 1218.
- [17] Jige, D., Sagawa, K., Iizuka, S., and Inoue, N., 2018, “Boiling Heat Transfer and Flow Characteristic of R32 Inside a Horizontal Small-Diameter Microfin Tube,” *Int. J. Refrig.*, **95**, pp. 73–82.
- [18] Jige, D., Iizuka, S., and Inoue, N., 2018, “Boiling Heat Transfer and Pressure Drop of R1234ze(E) Inside a Small-Diameter 2.5 mm Microfin Tube,” *International Refrigeration and Air Conditioning Conference*, West Lafayette, IN, July 9–12, p. 2542.
- [19] Jige, D., and Inoue, N., 2019, “Flow Boiling Heat Transfer and Pressure Drop of R32 Inside 2.1 mm, 2.6 mm and 3.1 mm Microfin Tubes,” *Int. J. Heat Mass Transfer*, **134**, pp. 566–573.
- [20] Diani, A., Mancin, S., and Rossetto, L., 2014, “R1234ze(E) flow Boiling Inside a 3.4 mm ID Microfin Tube,” *Int. J. Refrig.*, **47**, pp. 105–119.
- [21] Diani, A., Mancin, S., and Rossetto, L., 2015, “Flow Boiling Heat Transfer of R1234yf Inside a 3.4 mm ID Microfin Tube,” *Exp. Therm. Fluid Sci.*, **66**, pp. 127–136.
- [22] Diani, A., and Rossetto, L., 2015, “Vaporization Inside a Mini Microfin Tube: Experimental Results and Modeling,” *J. Phys. Conf. Ser.*, **655**, p. 012032.
- [23] Diani, A., Mancin, S., Cavallini, A., and Rossetto, L., 2016, “Experimental Investigation of R1234ze(E) flow Boiling Inside a 2.4 mm ID Horizontal Microfin Tube,” *Int. J. Refrig.*, **69**, pp. 272–284.
- [24] Longo, G. A., Mancin, S., Righetti, G., Zilio, C., and Doretti, L., 2017, “Saturated R134a Flow Boiling Inside a 4.3 mm Inner Diameter Microfin Tube,” *Sci. Technol. Built Environ.*, **23**(6), pp. 933–945.
- [25] Diani, A., Cavallini, A., and Rossetto, L., 2017, “R1234yf Flow Boiling Heat Transfer Inside a 2.4-mm Microfin Tube,” *Heat Transfer Eng.*, **38**(3), pp. 303–312.
- [26] Diani, A., and Rossetto, L., 2018, “Experimental Analysis of Refrigerants Flow Boiling Inside Small Sized Microfin Tubes,” *Heat Mass Transfer Stoffuebertrag.*, **54**(8), pp. 2315–2329.
- [27] Righetti, G., Longo, G. A., Zilio, C., Akasaka, R., and Mancin, S., 2018, “R1233zd(E) flow Boiling Inside a 4.3 mm ID Microfin Tube,” *Int. J. Refrig.*, **91**, pp. 69–79.
- [28] Longo, G. A., Mancin, S., Righetti, G., and Zilio, C., 2019, “R1224yd(Z) flow Boiling Inside a Mini Microfin Tube,” *Proceedings of the 25th IIR International Congress of Refrigeration*, Montréal, Canada, Aug. 24–30, p. 404.
- [29] Diani, A., and Rossetto, L., 2019, “R513A Flow Boiling Heat Transfer Inside Horizontal Smooth Tube and Microfin Tube,” *Int. J. Refrig.*, **107**, pp. 301–314.
- [30] Diani, A., and Rossetto, L., 2020, “Characteristics of R513A Evaporation Heat Transfer Inside Small-Diameter Smooth and Microfin Tubes,” *Int. J. Heat Mass Transfer*, **162**, p. 120402.
- [31] Lallemand, M., Branescu, C., and Haberschill, P., 2001, “Local Heat Transfer Coefficients During Boiling of R22 and R407C in Horizontal Smooth and Microfin Tubes,” *Int. J. Refrig.*, **24**(1), pp. 57–72.
- [32] Kim, Y., Seo, K., and Chung, J. T., 2002, “Evaporation Heat Transfer Characteristics of R-410A in 7 and 9.52 mm Smooth/Micro-Fin Tubes,” *Int. J. Refrig.*, **25**(6), pp. 716–730.
- [33] Yu, M., Lin, T., and Tseng, C., 2002, “Heat Transfer and Flow Pattern During Two-Phase Flow Boiling of R-134a in Horizontal Smooth and Microfin Tubes,” *Int. J. Refrig.*, **25**(6), pp. 789–798.
- [34] Wongs-Ngam, J., Nualboonrueng, T., and Wongwises, S., 2004, “Performance of Smooth and Micro-Fin Tubes in High Mass Flux Region of R-134a During Evaporation,” *Heat Mass Transfer Stoffuebertrag.*, **40**(6–7), pp. 425–435.
- [35] Spindler, K., and Müller-Steinhagen, H., 2009, “Flow Boiling Heat Transfer of R134a and R404A in a Microfin Tube at Low Mass Fluxes and Low Heat Fluxes,” *Heat Mass Transfer*, **45**(7), pp. 967–977.
- [36] Bandarra Filho, E. P., and Barbieri, P. E. L., 2011, “Flow Boiling Performance in Horizontal Microfinned Copper Tubes With the Same Geometric Characteristics,” *Exp. Therm. Fluid Sci.*, **35**(5), pp. 832–840.
- [37] Padovan, A., Del Col, D., and Rossetto, L., 2011, “Experimental Study on Flow Boiling of R134a and R410A in a Horizontal Microfin Tube at High Saturation Temperatures,” *Appl. Therm. Eng.*, **31**(17–18), pp. 3814–3826.
- [38] Han, X., Li, P., Wang, Z., Wang, X., Zhang, X., and Chen, G., 2013, “Evaporation Heat Transfer and Pressure Drop of R161 in a 7 mm Micro-Fin Tube,” *Int. J. Heat Mass Transfer*, **62**, pp. 638–646.
- [39] Kondou, C., Baba, D., Mishima, F., and Koyama, S., 2013, “Flow Boiling of Non-Azeotropic Mixture R32/R1234ze(E) in Horizontal Microfin Tubes,” *Int. J. Refrig.*, **36**(8), pp. 2366–2378.
- [40] Kondou, C., Mishima, F., Liu, J., and Koyama, S., 2014, “Condensation and Evaporation of R134a, R1234ze (E) and R1234ze (Z) Flow in Horizontal Microfin Tubes at Higher Temperature,” *International Refrigeration and Air Conditioning Conference*, West Lafayette, IN, July 14–17, p. 1446.
- [41] Kim, N. H., 2015, “Evaporation Heat Transfer and Pressure Drop of R-410A in a 5.0 mm O.D. Smooth and Microfin Tube,” *Int. J. Air-Cond. Refrig.*, **23**(1), pp. 1–15.
- [42] Jiang, G. B., Tan, J. T., Nian, Q. X., Tang, S. C., and Tao, W. Q., 2016, “Experimental Study of Boiling Heat Transfer in Smooth/Micro-Fin Tubes of Four Refrigerants,” *Int. J. Heat Mass Transfer*, **98**, pp. 631–642.
- [43] Yang, C. M., and Hrnjak, P., 2018, “Effect of Straight Micro Fins on Heat Transfer and Pressure Drop of R410A During Evaporation in Round Tubes,” *Int. J. Heat Mass Transfer*, **117**, pp. 924–939.
- [44] Kim, N. H., 2019, “Convective Boiling of R-410A in 5.0 and 7.0 mm Outer Diameter Microfin Tubes,” *Exp. Heat Transfer*, **33**(4), pp. 1–19.
- [45] Colombo, L. P. M., Lucchini, A., Phan, T. N., Molinaroli, L., Niro, A., and Pozzoni, M., 2020, “Saturation Temperature Effect on Heat Transfer Coefficient During Convective Boiling in Microfin Tubes,” *J. Phys. Conf. Ser.*, **1**(1), p. 1599.
- [46] Righetti, G., Longo, G. A., Zilio, C., and Mancin, S., 2019, “Flow Boiling of Environmentally Friendly Refrigerants Inside a Compact Enhanced Tube,” *Int. J. Refrig.*, **104**, pp. 344–355.
- [47] Collier, J. G., and Thome, J. R., 1994, *Convective Boiling and Condensation*, Oxford University Press, New York.
- [48] Se-Yoon, O., and Bergles, A. E., 2002, “Visualization of the Effects of Spiral Angle on the Enhancement of in-Tube Flow Boiling in Microfin Tubes,” *ASHRAE Trans.*, **108**(Part 2), p. 516.
- [49] Webb, R. L., Narayanamurthy, R., and Thors, P., 2000, “Heat Transfer and Friction Characteristics of Internal Helical-Rib Roughness,” *ASME J. Heat Transfer-Trans. ASME*, **122**(1), pp. 134–142.
- [50] Fukano, T., and Ousaka, A., 1989, “Prediction of the Circumferential Distribution of Film Thickness in Horizontal and Near-Horizontal Gas-Liquid Annular Flows,” *Int. J. Multiphase Flow*, **15**(3), pp. 403–419.
- [51] Cioncolini, A., and Thome, J. R., 2013, “Liquid Film Circumferential Asymmetry Prediction in Horizontal Annular Two-Phase Flow,” *Int. J. Multiphase Flow*, **51**, pp. 44–54.
- [52] Thome, J. R., Favrat, D., and Kattan, N., 1997, “Evaporation in Microfin Tubes: A Generalized Prediction Model,” *Proceedings of Convective Flow and Pool Boiling Conference*, Irsee, Germany, May 18–23.
- [53] Yashar, D. A., Wilson, M. J., Kopke, H. R., Graham, D. M., Chato, J. C., and Newell, T. A., 2001, “An Investigation of Refrigerant Void Fraction in Horizontal, Microfin Tubes,” *HVACR Res.*, **7**(1), pp. 67–82.
- [54] Koyama, S., Lee, J., and Yonemoto, R., 2004, “An Investigation on Void Fraction of Vapor-Liquid Two-Phase Flow for Smooth and Microfin Tubes With R134a at Adiabatic Condition,” *Int. J. Multiphase Flow*, **30**(3), pp. 291–310.
- [55] Kattan, N., Thome, J. R., and Favrat, D., 1998, “Flow Boiling in Horizontal Tubes: Part 2—New Heat Transfer Data for Five Refrigerants,” *ASME J. Heat Transfer-Trans. ASME*, **120**(1), pp. 148–155.
- [56] Wojtan, L., Ursenbacher, T., and Thome, J. R., 2005, “Investigation of Flow Boiling in Horizontal Tubes: Part II—Development of a New Heat Transfer Model for Stratified-Wavy, Dryout and Mist Flow Regimes,” *Int. J. Heat Mass Transfer*, **48**(14), pp. 2970–2985.
- [57] Kedzierski, M. A., and Kang, D., 2018, “Horizontal Convective Boiling of R1234yf, R134a, and R450A Within a Micro-Fin Tube,” *Int. J. Refrig.*, **88**, pp. 538–551.